Drift and mixing under the ocean surface revisited: Stratified conditions and model-data comparisons

Nicolas Rascle,[1, 2] and Fabrice Ardhuin,[1]

Nicolas Rascle, Centre Militaire d'Océanographie, Service Hydrographique et Océanographique de la Marine, 29609 Brest, France

[1]Centre Militaire d'Océanographie,
Service Hydrographique et Océanographique
de la Marine, 29609 Brest, France.

[2]Laboratoire de Physique des Océans,
Université de Bretagne Occidentale, 29000
Brest, France.

Abstract. A model of the ocean surface currents is presented. It includes the enhanced near-surface mixing due to the waves, the Stokes drift ~~of the waves~~, the Stokes-Coriolis effect and the stratification. ~~The~~ near-surface current shears from this model are compared with the shears of the quasi-Eulerian currents measured using a wave-following platform during the Shelf Mixed Layer Experiment (SMILE). It is shown that the downwind current shears observed during SMILE are well modelled. However, the observed crosswind shears are in poor agreement with the model. The Stokes-Coriolis (SC) term could qualitatively explain this misfit but it is one order of magnitude too weak. The Ekman-Stokes spiral of the model are compared to the spiral observed during the long time series of measurements Long Term Upper Ocean Study 3 (LOTUS3). The effects of stratification are carefully treated. The mean velocity profiles of the model closely agree with observations. However, we find no evidence of the SC effect on the shape of the observed Ekman spiral. The observed shape is found to be a consequence of the rectification due to the stratification. The SC effect calculated from an accurate numerical wave hindcast is weak, but should have been observed. In fact, it is estimated that the wave-induced bias in the current measurements is larger than the SC effect. Finally, it is shown that the wave age effect on the surface drift, which was found to be small in unstratified conditions, is important in the presence of shallow mixed layers.

1. Introduction

Waves are known to dramatically enhance the near-surface mixing. This was inferred from turbulent kinetic energy (TKE) dissipation measurements [*Agrawal et al.*, 1992; *Terray et al.*, 1996], and it was also observed in measurements of downwind current vertical shear very close to the surface during the Shelf Mixed Layer Experiment (SMILE) [*Santala*, 1991; *Terray et al.*, 2000]. Accordingly, the surface mean current is rather weak, around 0.5% of the wind speed at 10 meters U_{10} when the ocean is not stratified and when the waves are developed. This quasi-Eulerian mean current is defined as the Lagrangian drift minus the wave Stokes drift [see for details *Jenkins*, 1987; *Rascle et al.*, 2006; *Ardhuin et al.*, 2007b]. This small quasi-Eulerian drift can be overwhelmed by large surface drift due to the wave Stokes drift, which can be as large as 1.2% of U_{10} [*Rascle et al.*, 2006, hereinafter RAT06]. However, these processes may not be well represented or, more likely, other processes are important for the drift of surface-trapped buoyant objects to reach surface drifts of the order of 2 or 3% of U_{10} [*Huang*, 1979]. The surface trapping of the Ekman current in the presence of stratification may be an important factor.

Waves are also associated with a Stokes-Coriolis current [*Hasselmann*, 1970; *Xu and Bowen*, 1994~~; *McWilliams and Restrepo*, 1999~~]. Namely, in a rotating frame of reference, a wave-induced stress perpendicular to the waves propagation modifies the profile of the Ekman current. In an inviscid ocean, this stress drives a mean current which compensates the Stokes drift of the waves when averaged over the inertial period. However, in the presence of a strong vertical mixing, this return flow is made vertically uniform. Because the Stokes drift of a wind sea ~~is strongly surface trapped~~, the return flow only compensates the Stokes drift when vertically integrated over depth, and there is a net drift at every depth. This was shown in RAT06 without any stratification, a ~~the question raised is to which extend this remains valid if the Ekman current is also surface trapped, by a shallow mixed layer for instance~~.

~~Furthermore,~~ when considering vertically integrated transports, the Stokes-Coriolis effect does compensate the Stokes transport in a steady state. ~~It is also the only mechanism invoked to compensate it~~. Observations ~~have been made~~ by *Smith* [2006], which the modulations of the Stokes drift by the passing wave groups was completely compensated, presumably by the flow associated with long infra-gravity waves. We also note that laboratory measurements fail to reproduce the Stokes drift [*Monismith et al.*, 2007]. However, the steady Stokes transport and the Stokes-Coriolis effect on it have never been clearly observed yet, except very close to the shore from bottom-mounted ADCP's [*Lentz et al.*, 2007]. Evidence of this effect has been sought by *Lewis and Belcher* [2004] and *Polton et al.* [2005] in the observations of the sub-surface Ekman current during Long Term Upper Ocean Study 3 (LOTUS3) [*Price et al.*, 1987]. Unfortunately, neither the wave-enhanced surface mixing nor the quite shallow diurnal mixed layer during LOTUS3 have been taken into account in ~~the previous works of *Lewis and Belcher* [2004] and *Polton et al.* [2005]~~, although they can radically change the interpretation of the observed Ekman spiral [*Price and Sundermeyer*, 1999]. Also, evidence of the Stokes-Coriolis forcing have not been sought yet in measurements much closer to the surface, such as those of SMILE.

The present work ~~is built on the previous paper RAT06~~, which can be summarized as follows: ~~The main idea of~~ the ~~description of the~~ near-surface ~~dynamics~~ Flow is ~~the~~ separation ed

~~of the current~~ into a wave Stokes drift and a quasi-Eulerian current. Th~~at~~is physical description leads to a different analysis of the near-surface current measurements whether they are Lagrangian or Eulerian, because the Stokes drift was shown to be of same ~~magnitude~~ order ~~than~~ as the quasi-Eulerian current. Using a vertical-mixing model built to reproduce observed TKE dissipation rates below the surface, RAT06 made preliminary model-data comparisons of near-surface quasi-Eulerian currents and of sub-surface Eulerian hodographs, showing encouraging results. However, those comparisons ~~with current measurements were sketchy and~~ needed further analysis. For instance, the near-surface quasi-Eulerian currents observed during SMILE were only compared to model predictions in the downwind direction, ~~and were made using the quite constraining analysis of~~ *Santala* [1991] (see section 3). Also the effect of stratification was ~~missing~~ in RAT06, whereas it could change the hodograph interpretations as well as the conclusions drawn in terms of surface drift.

In this paper the effect of stratification will thus be added to the model presented in RAT06 in order to make a quantitative comparison with the observations of near-surface current, ~~More precisely the remaining issues are:~~ How well this model can reproduce the vertical shears observed close to the surface, both in the downwind and the crosswind direction? What is the impact of the Stokes-Coriolis effect on the Eulerian and Lagrangian current profiles in shallow mixed layers? Is there any observational evidence of this effect? ~~Is the surface drift reaching realistic values in the presence of shallow mixed layers?~~

The model used for this study is introduced in section 2. The near-surface shears of the quasi-Eulerian currents observed during SMILE are analyzed in section 3. The Ekman-

Stokes spirals from the LOTUS3 data are analyzed in section 4. Finally, the surface drift of the model in the presence of waves and stratification is discussed in section 5.

2. The model

The model used in the present study can be summarized as follows. Oceanic motions are separated in three components, mean flow, waves and turbulence. Turbulence is separated from other motions by a an average over flow realizations for given wave phases. The mean flow and wave motions are then averaged with a generalized ? Lagrangian mean so that the mean momentum is separated into a mean flow and a wave part. With ρ_w being the water density, the horizontal total mean momentum $\rho_w \mathbf{U}$ is split in a quasi-Eulerian mean $\rho_w \widehat{\mathbf{u}}$ and a Stokes drift,

$$\mathbf{U} = \widehat{\mathbf{u}} + \mathbf{U}_s. \tag{1}$$

The Stokes drift is calculated from a spectrum of the sea surface elevation, and is used as a forcing for the model of the ocean water column. Following *Ekman* [1905] we assume that the wave, velocity, and turbulent properties are uniform horizontally, which reduces the problem to the vertical dimension.

For the sake of simplicity and because we want to simulate a period of hundreds of days, a simple eddy viscosity model with a TKE closure scheme will be used. This model is adapted from *Craig and Banner* [1994], as discussed in RAT06. It was chosen because it is able to reproduce the wave-enhanced near surface mixing by the addition of a TKE flux at the surface and the specification of a large roughness length z_0. The extension to a stratified ocean is taken from *Noh* [1996] and following works [*Noh and Kim*, 1999; *Noh*, 2004]. The parameterization of the effects of stratification on the eddy diffusivities is made via a turbulent Richardson number, where the destruction of turbulence by stratification is made regardless of the origin of turbulence, by shear production or by downward diffusion from the wave layer. This model was chosen for its ability to reproduce the diurnal thermocline.

The equations for the quasi-Eulerian horizontal momentum, for the mean buoyancy $B = -g\rho_w/\rho_0$ (g is the gravity acceleration and ρ_0 a reference density) and for the mean turbulent kinetic energy E write [*Noh and Kim*, 1999]

$$\frac{\partial \widehat{\mathbf{u}}}{\partial t} = -f\mathbf{e}_z \times (\widehat{\mathbf{u}} + \mathbf{U}_s) + \frac{\partial}{\partial z}\left(K\frac{\partial \widehat{\mathbf{u}}}{\partial z}\right), \tag{2}$$

$$\frac{\partial B}{\partial t} = \frac{\partial}{\partial z}\left(K_B\frac{\partial B}{\partial z}\right), \tag{3}$$

$$\frac{\partial E}{\partial t} = \frac{\partial}{\partial z}\left(K_E\frac{\partial E}{\partial z}\right) + K\left(\frac{\partial \widehat{\mathbf{u}}}{\partial z}\right)^2 + K_B\left(\frac{\partial B}{\partial z}\right) - \frac{Cq^3}{l}, \tag{4}$$

where $q = \sqrt{2E}$ is the turbulent velocity scale, l is the mixing length, and where we used the eddy viscosity and diffusivity concepts. Those viscosity and diffusivities are parameterized by

$$(K, K_B, K_E) = lq\,(S, S_B, S_E)\,. \tag{5}$$

The proportionality constants (S, S_B, S_E, C) depend on the stratification via the introduction of a turbulent Richardson number [*Noh*, 2004]

$$Ri_t = \left(\frac{Nl}{q}\right)^2, \tag{6}$$

$$S = 0.39\,(1 + 5Ri_t)^{-1/2}\,, \tag{7}$$

$$S_B = S/0.8\,(1 + 0.5Ri_t)^{1/2}\,, \tag{8}$$

$$S_E = S/1.95, \tag{9}$$

$$C = 0.39^3\,(1 + 5Ri_t)^{1/2}\,, \tag{10}$$

where N is the Brunt-Väisälä frequency ($N^2 = -\partial B/\partial z$). Note that all proportionality constants (S, S_B, S_E, C) depend on the the turbulent Richardson number Ri_t and that the buoyancy diffusivity adds a Prandtl number which also depends on Ri_t.

The mixing length is parameterized as

$$l = \frac{\kappa(z_0 - z)}{1 + \kappa(z_0 - z)/h}, \tag{11}$$

where $\kappa = 0.4$ is the von Kármán's constant, h is the mixed layer depth (defined as the depth where the TKE is reduced by four orders of magnitude compared to its surface value [*Noh*, 2004]) and z_0 is a roughness length, set to $z_0 = 1.6 H_s$ as in *Terray et al.* [2000]. H_s is the significant wave height of the wind sea, a proxy for the scale of the breaking waves that are responsible for the mixing.

The boundary conditions at the mean sea level ($z = 0$) are

$$K \frac{\partial \widehat{\mathbf{u}}}{\partial z}|_{z=0} = u_*^2, \tag{12}$$

$$K_B \frac{\partial B}{\partial z}|_{z=0} = Q \tag{13}$$

$$K_E \frac{\partial E}{\partial z}|_{z=0} = \Phi_{oc}, \tag{14}$$

where u_* is the waterside friction velocity, Q is the surface downward buoyancy flux and Φ_{oc} is the surface downward TKE flux. According to *Terray et al.* [1996], the TKE flux is parameterized as $\Phi_{oc} = \alpha u_*^3$, with $\alpha = 100$.

The bottom has almost no effect on the near surface dynamics, provided that the depth is substantially greater than the depth reached by the Stokes drift, than the Ekman depth and than the mixed layer depth. Therefore, the bottom boundary layer is not described here.

Those equations are solved with a time step of $dt = 10$ s and a vertical discretization of $dz = 1$ m. Each variable are collocated, the space differentials are expressed in standard second order centrally differenced forms and the time step is implicit.

Justification for the use of such a simple eddy viscosity model can be found by comparing the velocity profiles of the model to the velocity profiles of more sophisticated models like the large eddy simulations (LES) of *McWilliams et al.* [1997] or *Noh et al.* [2004]. Such comparisons have shown reasonable agreement [e.g. *Kantha and Clayson*, 2004].

3. Analysis of the near-surface shears - The SMILE data

3.1. The experiment

The SMILE experiment was described in details by *Santala* [1991], the reader is referred to his PhD thesis for additional information while only a short review will be given here. The SMILE experiment took place on the northern California shelf in 1988-1989. It included measurements of oceanographic and atmospheric variables from moored instruments. One measurement is of particular interest because one buoy, the Surface Acoustic Shear Sensor (SASS), included measurements of the velocity very close to the surface, at depths smaller than H_s. In our analysis, we will focus on those SASS measurements, ignoring the longer and deeper measurements from conventional moorings made during the same field experiment and we will use the abbreviation SMILE to refer to the SASS measurements only. The SASS buoy is a rigid array designed specifically to follow the surface elevation. It was moored over the shelf in 90 m depth, at the location (38°39′ N, 123°29′ W). The currents relative to the buoy was measured at depths 1.11, 2.51, 3.11 and 5.85 using 4 acoustic current meters. Gyroscopes and accelerometers were used to measure the motion of the buoy relative to the inertial frame of reference. The resulting measurements of currents referred to the inertial frame are unique with respect to their proximity of the surface. The currents were averaged over 40 mn. Horizontal average velocities were corrected for a wave bias due to correlations between the SASS motion and the wave orbital velocities, estimated from measured wave spectra (see also section 4.6 for a physical description of the wave bias). The velocities were also corrected for estimated errors due to flow disturbance induced by the structure.

The most useful measurement is a set of 13 time averages over 40 mn, spread during the afternoon and night on 27th February 1989. The average wind speed was $U_{10} = 13.6$ m s^{-1} and the average wave height was $H_s = 2.3$ m, both approximately aligned (from the North West, 300°) and steady. The wave peak period was $T_p = 7.8$ s, which corresponds to a wave age $C_p/U_{10} = 0.89$, where C_p is the wave phase speed at the spectral peak. The combined measurements of temperature with the SASS and with the nearby conventional mooring show that water column was unstratified until a depth of 20 m. To parameterize the atmospheric boundary layer, *Santala* [1991] used local observations and extrapolated missing observations, such as the air temperature, from distant buoy measurements. He calculated the stability parameter $-\kappa Z/L$ [*Large and Pond*, 1981], where $Z = 7$ m is the elevation above the sea surface and $L = u_*^3/Q$ the Monin-Obukhov length scale, and obtained values comprised between 0 and -0.03. The corresponding downward surface heat flux Q_h is thus between 0 and -8 W m^{-2}. Using a similar combination of in-situ measurements and bulk formulae, *Beardsley et al.* [1998] found that the shortwave heat flux roughly compensates the longwave, latent and sensible heat loss, giving a small daily mean surface heat flux on February 27-28, around +30 W m^{-2} given the uncertainty of visual reading of *Beardsley et al.* [1998]'s fig. 6. Such a small heat flux is certainly of minor importance with respect to the strong wind forcing, as shown by the large values of the Monin-Obukhov length scale (93 m). This allows us to simply suppose that the surface heat flux was nil during the experiment.

3.2. The model

For comparison with these data, the model is run with a steady wind of the observed wind speed. The temperature is initialized to fit the observed profile, with a thermocline around 20 m, and a zero surface heat flux is used. To compute the Stokes-Coriolis force, waves are calculated using a JONSWAP spectrum [*Hasselmann et al.*, 1973; *Kudryavtsev et al.*, 1999], assuming a fetch of 100 km which gives the observed H_s. The peak period of waves is slightly underestimated with this method, giving $T_p = 6.4$ s whereas 7.8 s was observed. The Stokes transport of the waves, important to measure the magnitude of the Stokes-Coriolis force, might then be slightly overestimated. The model results, averaged over an inertial period, are plotted on fig. 1 (upper panel). For comparison, the model results without stratification are plotted on fig. 1 lower panel.

3.3. Previous analysis

The measurements have already been analyzed by *Santala* [1991], and part of its results were used by *Terray et al.* [2000] and in RAT06. Here we will briefly summarize their analysis and the different technique used in the present analysis.

Four sensors were mounted on the SASS buoy, at depths from 1 to 5m. The vertical shear can be estimated between each pair of adjacent sensors by a finite difference. *Santala* [1991] scaled the depth with u_*^2/g, which is equivalent to scale with the significant wave height H_s if one supposes a full development and if one omits the swell in H_s. The shear was scaled with u_*/z, the law of the wall scaling. This leads to their figure 7-5, which we reproduce here for the SASS data only (fig. 2).

The analysis of this plot, together with deeper measurements from a conventional mooring, leads these authors to infer a description of the downwind shear in a 3 layer structure, namely an upper layer with almost no shear, a lower layer following a log-law and a transition layer in between. However, such a transition is hardly perceptible with only the SASS data, because the lowest shear estimate falls in the transition region (fig. 2, upper panel). In the crosswind direction, the shear was found roughly constant with depth. This analysis leads to the figure 7-11 in *Santala* [1991], which was reproduced in *Terray et al.* [2000] and RAT06, showing the current profiles inferred from this analysis. These profiles were used afterwards in the discussion of *Santala* [1991].

3.4. A less constraining analysis

It is not obvious from fig. 2 that the fit to the scatter of finite difference calculated shears should produce a reliable estimation of the mean shear. Given that large scatter, one can wonder if a different analysis of the shears close to the surface cannot lead to a different description of the near surface velocity profiles. For instance, since we are focusing our analysis on the near-surface, where the mixing is enhanced by the waves, the shear should better be scaled with u_*/H_s or g/u_*, according to *Craig and Banner* [1994]'s eq. 30. But whatever the scaling used for the depth or for the shear, vertical profiles of shear calculated by finite difference remain quite noisy (fig. 3).

A smoother estimation of the mean vertical shear can be obtained with a linear regression of the current profile over the 4 sensors depths. The choice of a linear profile, instead of a logarithmic one, corresponds to the constant near-surface shear expected in the wave-stirred layer, as mentioned above [see *Craig and Banner*, 1994, equ. 30]. By imposing the vertical structure of the shear, this estimation method avoids the spreading due to finite difference shear estimations. It also reduces drastically the scatter between the 13 time measurements, as shown in fig. 4.

The observed and modelled shears are shown in fig. 5, with the elevation scaled by H_s and the current by u_*. In the downwind direction (fig 5, upper panel) the observed shear, scaled by u_*/H_s, is 0.42 (0.26), where the first number is the mean and the number in parentheses is the standard deviation. The corresponding downwind shear of the model is 0.23 with the full model. If the wave-enhanced near-surface mixing is omitted in the model (by using a small roughness length $z_0 = 5$ cm and by setting the TKE surface flux to zero), the shear reaches 1.52. As was noted in *Terray et al.* [2000] and RAT06, those observations of quite weak near-surface downwind shears are consistent with an intense wave-induced mixing.

In the crosswind direction (fig. 5, lower panel) the mean non-dimensional observed shear is -0.52 (0.31). The corresponding crosswind shear of the full model is -0.030, which is one order of magnitude smaller than the observations.

The Stokes-Coriolis force, oriented in the crosswind direction, is a possible explanation for that large observed crosswind shear. Qualitatively, the Stokes-Coriolis force is a good candidate, because it is oriented to the right of the waves propagation, as is the observed shear bias. Therefore we made a quantitative evaluation of the Stokes-Coriolis impact on the crosswind current. The wave field was not fully developed. The Stokes transport is around 10% of the Ekman transport, which means, according to *Polton et al.* [2005], that the Stokes-Coriolis effect is equivalent to a surface stress of 10% of the wind stress.

The consequent crosswind shear (fig 5, lower panel) is quite small, increasing from −0.014 without the Stokes-Coriolis force to −0.030 with it. An upper bound of the Stokes-Coriolis stress can be found by supposing the wave field fully developed. The equivalent stress is then of 35% of the wind stress. But even in this case, the crosswind shear only reaches −0.041 (fig. 5, lower panel). The Stokes-Coriolis force is too weak to explain the large crosswind observed shears, and this is a consequence of the strong wave-induced mixing imposed in the model. Namely, if we omit the wave-induced mixing in the model, the crosswind shear reaches −0.21 without the Stokes-Coriolis force, −0.31 with it and even −0.37 when supposing maximum value of the Stokes-Coriolis force, in better agreement with the observed shear. Clearly, the SMILE observations of crosswind shear do not validate any wave-induced enhancement of the mixing, whereas the downwind observations did.

The possible explanation for those shear observations is a smaller mixing in the crosswind direction (fig. 5, lower panel) than in the downwind direction. Such phenomenon appears hardly plausible when dealing with wave-breaking induced turbulence, because the turbulence generated is likely to be isotropic. This is not the case for Langmuir turbulence. From looking at the vertical profiles of different LES simulations of Langmuir turbulence (*McWilliams et al.* [1997], *Noh et al.* [2004],...), it is clear that the mixing due to Langmuir cells is not isotropic. However none of these simulations are focused enough on the near-surface dynamics to provide any reliable picture of what the mean surface currents and mixing should be.

Also, if Langmuir circulations were present, the SASS buoy could have been trapped into surface convergence zones. *Santala* [1991] investigated the vertical velocity records and did find a non-zero mean downward velocity, interpreted as evidence of a non-uniform sampling of the Langmuir cells. The consequent bias on the horizontal velocity measurement cannot be excluded to explain the large observed crosswind shear.

4. Analysis of the current magnitude - The LOTUS data

The impact of the Stokes-Coriolis effect and of the stratification is small on the current shear, but is more apparent on the magnitude of the current : the Ekman transport is trapped in the mixed layer, leading to large values of the crosswind current, while the Stokes-Coriolis effect gives small values, if not negative, of the downwind current (see e.g. fig. 1, upper panel). Are the observed current in agreement with that expected shape?

Field measurements of the Ekman currents always include a lot of noise, which finds its origins in inertial oscillations and in the diverse transient phenomenons, some of them being surface-trapped. It is thus difficult to separate other processes from the mean wind-driven current. During SMILE (previous section), the currents were averaged over 40 mn. This allows an analysis of the vertical shears but it is insufficient to investigate the magnitude of the current. One solution to get rid of this noise is to average the current over a long time period. This method has been employed by *Price et al.* [1987] with the LOTUS3 data set.

The LOTUS3 measurement took place in the western Sargasso Sea (34.0N, 70.0W) in the summer of 1982, under light to moderate winds, $U_{10} = 5.4$ (2.7) m s^{-1}, and strong diurnal heating. The current measurements came from Vector Measuring Current Meters (VMCMs) along a conventional mooring, with the upper measurements at 5, 10, 15 and 25 m depth. In the typical light wind encountered, the waves were not really large, $H_s = 1.3$ (0.7) m, so that the wave bias, i.e. the correlation between the motion of the mooring and the orbital motion of the waves, was first estimated to be small at the measurement depths using VMCMs [*Schudlich and Price*, 1998]. We will further discuss this point below. Finally *Price et al.* [1987] used a coherent averaging method to follow the low frequency changes in wind direction. The resulting current profile can then be quantitatively compared to theoretical models of the Ekman current. This observed current has the expected profile of an Ekman spiral, with a depth integrated transport in agreement with the Ekman transport. However some features of this current were unexpected. First, the sub-surface deflection is quite large, around 75° at a depth of 5 m. Second, the decay with depth is stronger than the clockwise rotation (the spiral is 'flat').

To explain this flatness of the spiral, *Price and Sundermeyer* [1999] invoked the temporal variation of stratification. The mixed layer depth varied typically from 10 m during the day to 25 m at night. The mean current, time-averaged over the diurnal cycle, should then show a different vertical profile than the current inferred from the mean vertical stratification. This difference is a problem of rectification of the Ekman layer [see e.g. *McWilliams and Huckle*, 2006].

However, *Lewis and Belcher* [2004] reported potential problems in this interpretation. Mainly, the approach of *Price and Sundermeyer* [1999] is not able to reconcile the observed large sub-surface deflection of 75° and a small surface deflection of 10 to 45° typically observed [*Huang*, 1979]. *Lewis and Belcher* [2004], followed by *Polton et al.* [2005], argued that the Stokes-Coriolis force can explain the large sub-surface deflection, together with a small surface deflection. The agreement between their models and the LOTUS3 observations is then quite good.

Other problems appear in turn in these models. First, the small surface deflections reviewed in *Huang* [1979] partly comes from observations of Lagrangian surface drift. As noted in RAT06, the Lagrangian surface drift is the sum of the Stokes drift and the quasi-Eulerian current. A large surface deflection of the quasi-Eulerian current is not contrary to a small surface deflection of the Lagrangian drift, because of the Stokes drift. In relation to this, the surface mixing in the models of *Lewis and Belcher* [2004] and *Polton et al.* [2005] is likely to be several orders of magnitude too small. But, as noted in RAT06 without stratification, a realistic surface mixing gives a quasi-Eulerian current much more uniform than modelled by the previous authors, ruining the agreement with the data (see RAT06, fig. 7). Stratification is therefore needed to reexamine the LOTUS 3 data. Here we also reexamine whether or not the LOTUS 3 data offer an observational evidence of the Stokes-Coriolis effect on the Ekman current.

4.1. A simple model of the diurnal cycle

Following the idealized model of *Price and Sundermeyer* [1999], the present model is run with the mean wind stress observed during the period, $u_* = 0.0083$ m s^{-1}. The waves are expected to be fully developed with that wind stress, which gives a significant wave height of $H_s = 1.6$ m, based on the JONSWAP spectrum [*Hasselmann et al.*, 1973].

The temperature is initialized with the temperature observed at the beginning of the field experiment. For the surface heat flux, we use an analytical fit of the solar insolation measured during clear sky days and we suppose that a steady heat loss equilibrates the surface heat budget,

$$Q = \max\left(0, 1000 \cos\left(\frac{2\pi t}{T_{day}}\right)\right) - \frac{1000}{\pi}, \tag{15}$$

where t is the time and T_{day} is a period of one day.

The mixed layer depth h is calculated using the model criteria $E(h) < E(z=0) \times 10^{-4}$. The probability density function (PDF) of the mixed layer depth is shown in fig. 6, showing a bipolar distribution corresponding to diurnal and nocturnal mixed layers. With those mean wind stress, surface heat flux and initial temperature, the mixed layer depth varies between 8 m and 40 m. Those values are same order of magnitude than the observed stratification during LOTUS3 (fig. 6). However the vertical profile of the current do not look like the observed current profile. The current of the model is too large and too much homogeneous within the mixed layer (fig. 7).

The velocity profile is not well reproduced when we use the mean wind stress, and it is not surprising. The rectification over sub-periods with weak wind should not leave a mean velocity profile homogeneous in the upper 8 m. Similarly, if a strong wind event occurred during the period, its effect must be apparent on the mean velocity profile below 30 m deep.

4.2. A more elaborate model: using the wind history

The previous results using the average wind stress are encouraging but the profile of the mean current exhibits a large sensitivity to the mixed layer depth history. The temperature variability is not well reproduced with only a simple reproduction of the diurnal cycle. We will therefore attempt a more realistic simulation of the LOTUS3 data, using the full historic of the wind stress.

Since there is no clear indication of what the damping of the inertial oscillations should be in a one dimensional model [e.g. *Mellor*, 2001], the wind is supposed to blow in a constant direction, in agrement with the coherent averaging of *Price et al.* [1987]. The bulk formulation of COAMPS (Patrick Marchesiello, personal communication) for the atmospheric boundary layer is used to calculate the wind stress. The relative humidity is set to 75%, as in *Stramma et al.* [1986]. The wind stress is set to the 6 hours low-pass filtered calculated wind stress, updated every 15 mn. Using the filtered wind stress and not the filtered wind speed conserves the stress and minimizes the rectification errors. Finally, the current of the model, averaged over one hour, is stored and used to calculate the mean over the whole time period (170 days).

When one wants to reproduce the stratification, both the heat budget and the large scale advection of heat come into play. Attempting to validate their 1D model of the ocean vertical mixing, *Gaspar et al.* [1990] analyzed a 2 weeks subset of the LOTUS 3 measurements. They reported imbalance of the order of 80W m^{-2} in the ocean heat budget. They estimated large scale advection to be responsible for an imbalance of 15W m^{-2}. Remaining errors were attributed to the bulk derived heat fluxes and uncertain estimations of latent heat flux [see *Stramma et al.*, 1986] and of solar infrared flux, due to missing measurements of relative humidity and of cloud type, respectively.

Those problems of advection and heat flux uncertainties are of critical importance for a simulation of the observed temperature, as the model temperature might slowly drift away from observations. However the present study focus on the current, for which the mixed layer depth is more important than the absolute value of the temperature. One can thus wonder if the use of the analytical heat flux (15) and of the observed wind stress are not enough to produce adequate mixed layer history. During day time it is enough (fig. 6), as the thickness of the diurnal mixed layer is determined by the Monin-Obukhov length scale, i.e. by the surface heat and momentum fluxes. However, the nocturnal convection and its effect on stratification is also determined by the temperature profile and the water column heat content, especially when the nocturnal heat loss exceeds the preceding diurnal heat gain. The small drift of the model temperature, when attempting a long time simulation of the LOTUS 3 experiment with the analytical heat flux (15), leads to large over-estimations of nocturnal mixed layer depth predictions (fig. 6).

4.3. A pragmatic model: Constraining the stratification

As surface flux and advection of heat are uncertain, and as the goal of the present paper is not to perform a temperature simulation but rather to compute the effect of stratification on current, we will avoid mixed layer depth errors by constraining the temperature to the observed temperature. A first simulation re-initializes every 6 hours the temperature of the model to the 1-hour mean observed temperature. The analytical fit (15) for the heat flux is still used to reproduce the high-frequency diurnal cycle. The temperature of the simulation is therefore in close agrement with the observed temperature (correlation coefficient above 0.99 at every measurement depth), including the diurnal stratification, except during a few episodes of exceptionally weak solar insolation not captured with our simple heat flux (15). As a consistency check, a second simulation uses a nudging of the temperature to the 6 hours low-pass filtered observed temperature. The time scale of the nudging is 1000 s. The temperature of this second simulation is also very close to the observed temperature (correlation coefficient above 0.99 at every measurement depth), except that the diurnal warming is somewhat weakened by the nudging. Those 2 simulations with constrained temperature are compared in term of mixed layer depth prediction, exhibiting small differences (a bias of 1.2 m, which is small given our vertical resolution and the criteria on the TKE reduction), so that only one PDF is shown in fig. 6.

Those similar mixed layer depths between the different methods validate the reproduction of the impact of the stratification on the current.

4.4. Model results

The comparison between the modelled current averaged over the entire period and the coherent averaging of observations by *Price and Sundermeyer* [1999] is very good (fig. 7 and 8). The crosswind current agrees well with the observations, with differences less than 0.36 cm s^{-1} ($= 0.45u_*$) and relative errors of less than 10% for the 3 upper measurements. The crosswind transport of the model is equal to the Ekman transport, corresponding to the mean wind stress, while the crosswind transport calculated with a trapezoidal extension of the data is slightly (8%) inferior [see also *Price et al.*, 1987]. The downwind current of the model, if we omit the Stokes-Coriolis effect, is in correct agreement with the observations, with differences less than 0.47 cm s^{-1} ($= 0.58u_*$) which still represent relative errors of the order of 100%. The downwind transport of the model without the Stokes-Coriolis effect is nil, and the downwind transport from the extrapolated data is around -1.9×10^{-3} m^2 s^{-1}, which is 0.26% of the crosswind Ekman transport.

Such agreement between the model and the observations is encouraging. It provides the opportunity to check the sensitivity to the different parameterizations of the model. In particular, one may wonder if the mean current profiles observed during LOTUS 3 are useful to check the wave-induced mixing parameterization.

We tested the model sensitivity to the roughness length. As shown in fig. 7, the mean velocity profile is mainly determined by the stratification and the consequent rectification effect. The wave-induced mixing is less discernable on velocity measurements below 5 m depth than above, and at those depth it is hard to discriminate between small and large values of the roughness length.

4.5. The Stokes-Coriolis effect

The Stokes drift has been calculated by supposing the wave field fully developed with the corresponding wind averaged over 6 hours. This gives an upper bound of the Stokes-Coriolis effect (fig. 8, dotted line).

A more realistic estimation of that effect is also needed. The complete historic of the waves during the period is preferable, because it includes possible correlations between large wave events, strong wind events and particular stratification events like deep mixed layers. Therefore, a global wave model of 1° resolution is used to produce the sea state at the LOTUS3 station (34.0N, 70.0W). The wave model is based on the WAVEWATCH III (WW3) code [*Tolman et al.*, 2002], in which the wind-wave evolution parameterizations have been replaced by those of *Bidlot et al.* [2005]. Although these parameterizations still have some problems in costal and swell-dominated areas [*Ardhuin et al.*, 2007a], they provide good results for the mean parameters H_s and T_{m02} when compared to the North Atlantic buoys measurements [*Ardhuin and Le Boyer*, 2006; *Rascle et al.*, 2008, Jean Bidlot personal communication]. This model is forced with 10-m winds 6-hourly analysis from the European Center for Medium-Range Weather Forecasting (ECMWF). The comparison with the nearby buoy 41001 (34.7N, 72.7W) of the National Data Buoy Center (NDBC) shows an rms error of 0.43 m on H_s (25% of the rms H_s) and of 0.57 s on the mean period T_{m02} (9.8% of the rms T_{m02}), for the period from 14 May to 30 November 1982. Note that no wave data were available at that buoy from 6 June to 6 August. Our calculation might underestimate the Stokes transport since there is a significant negative bias on the wave height H_s (-0.25 m), and a negligible bias on the mean period T_{m02} (-0.07 s).

The wave spectra at the LOTUS3 station were used to compute the Stokes drift. Consistently with the average of *Price et al.* [1987] which follows the wind direction, we need to rotate the Stokes drift components according to the wind rotation. To avoid any discrepancy between the observed wind direction and the reanalyzed wind direction, we need to use the ERA40 wind direction. Because at the surface the Stokes drift is a high moment of the spectrum, it is almost aligned with the wind. For computational simplicity, this surface Stokes drift direction is taken as a proxy for the ERA40 wind direction. Furthermore, the average of the Stokes drift (rotated following the wind rotation) over the whole time period is found to be aligned with the wind, with a mean crosswind Stokes transport of 2.3% of the downwind Stokes transport. It means that the mean contribution of waves not aligned with the wind, swell for instance, is weak. For additional simplicity, we thus use the norm of the Stokes drift and prescribe it aligned with the wind at each depth at every time step. This second simplification leads to an increase of the mean downwind Stokes transport by 2.6%, which is negligible compared to the uncertainties on the significant wave height reanalysis.

The numerical results with that estimation of the Stokes-Coriolis term are shown in fig. 8. The mean Stokes transport is 0.075 m^2 s^{-1}, i.e. 9.5% of the Ekman transport which reaches 0.79 m^2 s^{-1}. Accordingly, the mean downwind current transport of the model with the Stokes-Coriolis effect is -0.91 m^2 s^{-1}, which compensates the Stokes transport (within a 17% error which origin, from vertical insufficient dicretization or from rectification, is unknown). On the contrary the downwind transport from the extrapolated data is almost nil (-1.9×10^{-3} m^2 s^{-1}).

Similarly, the downwind current profile of the model is closer to the data when we omit the Stokes-Coriolis term (fig. 8). In this regard, the present work is consistent with the work of *Price and Sundermeyer* [1999], showing that the 'flatness' of the spiral results from the stratification, contrary to *Polton et al.* [2005] which claimed it results from the Stokes-Coriolis effect.

4.6. The wave bias

One explanation emerges for that apparent misfit of the model when including the Stokes-Coriolis effect: the nearly zero observed downwind transport was supposed to be Eulerian but could have been contaminated by the wave-induced buoy motion. Namely, the mooring line measured 5395 m in 5366 m of water and was then very taut. One can then consider that the sub-surface currentmeter motion follows the buoy motion, and this possibly leads a wave bias due to correlations between orbital wave motion and currentmeter motion. *Schudlich and Price* [1998] used the method of *Santala* [1991] to discuss that wave bias. In particular, one can suppose that the buoy moves vertically with the surface. Then, for each monochromatic wave train, one gets in addition to the quasi-Eulerian current a bias equal to

$$u_{bias}^{min}(z) = \frac{1}{2} a^2 \omega k \exp(-kz), \tag{16}$$

where z is the elevation measured downward, a is the wave amplitude, ω is the radian frequency and k the wavenumber. This gives a lower bound of the wave-bias. If one supposes that the buoy moves both vertically and horizontally, then one gets an upper-bound of the wave-bias

$$u_{bias}^{max}(z) = a^2 \omega k \exp(-kz). \tag{17}$$

For comparison, the Stokes drift of a monochromatic wave is

$$U_s(z) = a^2 \omega k \exp(-2kz). \tag{18}$$

As the wave-induced motions of the current meters are larger than the wave-induced motions of the particles, the maximum bias is larger than the Stokes drift (the equality arises at the surface only, see fig. 9, left panel).

We used the spectrum predicted by the wave model to compute the average over the whole LOTUS 3 period of u_{bias}^{min} and u_{bias}^{max} (fig. 9, left panel). Those wave bias have also been added to the downwind current of the model with the Stokes-Coriolis effect (fig. 9, right panel, thin lines).

The vertical integral of the bias is bounded by

$$M^w \leq \int_{-H}^{0} u_{bias} dz \leq 2M^w, \tag{19}$$

where M^w is the Stokes transport ($= a^2\omega/2$ for a monochromatic wave). Therefore, as the theoretical downwind transport is equal to $-M^w$, the biased transport is comprised between 0 and $+M^w$ (fig. 9, right panel, thin lines). The observed downwind transport in LOTUS 3 is approximately zero. It was interpreted by *Price et al.* [1987] as an evidence that the Ekman transport is crosswind. But the transport induced by the Stokes-Coriolis effect is not negligible (9.5% of the Ekman transport) and should have been observed. We argue here that it was not observed because of the wave bias. Furthermore, in the winter measurements of LOTUS 4, a positive downwind transport was found and was interpreted by *Schudlich and Price* [1998] as a wave bias, coming from the large winter waves. The present description supports the more nuanced conclusion that both the LOTUS3 and the LOTUS4 measurements are likely biased by the waves in the downwind direction.

5. Surface drift

One aim of the present model is a better understanding of the surface Lagrangian drift, for applications to search and rescue, fish larvae recruitment or any other studies following floating materials. The present model, following *Garrett* [1976] and *Jenkins* [1989], separates the flow into a wave Stokes drift and an Eulerian current. In particular, the introduction of the wave age should bring new insight in the near-surface dynamics. One remarkable result obtained in RAT06 for unstratified conditions is that the surface drift is almost independent of the wave age : as the waves gets more mature, the Stokes drift increases. But the mixing is also more efficient and leaves an Ekman current more homogeneous, thus reducing the surface quasi-Eulerian current and compensating the increase of the Stokes drift. This result is recalled in fig. 10 (upper panel, for $Q_h = 0$; note that the quasi-Eulerian current is weaker at the surface compared to results obtained in fig. 12 in RAT06 due to the poorer vertical resolution, the first level being at -0.5 m in the present model).

Whereas the wave age is a key parameter for the near-surface mixing, it has little influence on the surface drift. A simple parameterization of the surface drift directly from the wind might then be possible. Does this result extends to stratified conditions?

The dependance of the surface drift on the wave age in the presence of strong stabilizing buoyancy flux ($Q_h = 1000$ W m^{-2}, which gives a Monin-Obukhov length scale $L = 0.24$ m) is shown in fig. 10. For strong buoyancy forcing, the mixed layer is shallow (around $8-12$ m) so that the quasi-Eulerian surface current is almost crosswind (angle around

$-90°$). Consequently, the reduction of the quasi-Eulerian current, when waves get more developed and mixing more efficient, is not compensated by the increase of the Stokes drift of the waves, contrary to what happens in unstratified conditions where the angle between the Stokes drift and the quasi-Eulerian current is more modest (angle around 45°). In addition, the mixed layer of the model gets thicker with a larger wave-induced mixing (from 8 m for $Q_h = 0$ to 12 m for $Q_h = 1000$ W m^{-2}), which increases furthermore the wave age dependance of the surface drift during strong heating events. The surface drift thus reaches 3% of the wind speed U_{10} for very shallow mixed layer associate with small fetch. That mixed layer depth dependency on the wave age is physically sound but requires further verifications. This requires a full coupling of the mixed layer with the wave forcing, a task that is beyond the scope of the present study and is left for future work.

6. Conclusion

A model of the surface layer of the ocean was presented in RAT06. Essentially, the current was separated into a wave Stokes drift and a quasi-Eulerian current. That physical description leaded to a different analysis of the observations of currents profiles close to the surface, whether the measurements are Eulerian or Lagrangian. That analysis agreed qualitatively with a few available data of Lagrangian drift profiles, of Eulerian velocity profiles and of TKE dissipation rates. Motivated by these results, we added the stratification to the model of RAT06 and tried a more quantitative validation of the current profiles.

We performed a reanalysis of the near-surface quasi-Eulerian velocity measurements during SMILE. The near-surface shears were previously investigated by comparison to shears at greater depths obtained with an additional buoy [*Santala*, 1991], and the hypothesis of a 3 layer structure was made. Here we made no hypothesis on the structure of that shear and we linearly interpolate the upper current measurements. The near-surface shears obtained are found to be in good agreement with the downwind shears expected in the presence of a strong wave-induced mixing. However, crosswind shears found are an order of magnitude larger than expected. The Stokes-Coriolis force (or Hasselmann force) appeared as a good candidate but is one order of magnitude too weak to produce such shears. Consequently, the physics of the present model is not sufficient to explain the observed shears. Models and complementary observations of Langmuir cells appear therefore to be necessary for further investigations of these near-surface current measurements.

The long term observations of Ekman spirals during LOTUS 3 provide an opportunity to investigate the Stokes-Coriolis effect. The use of a long time series reduces the noise in the measurement, enabling an analysis of the magnitude of the wind-driven current. However, it introduces rectification effects because of the temporal variations of the wind and of the stratification. The wind variability is taken into account by using the coherent averaging of *Price et al.* [1987], which follows the wind direction, and changes in the stratification are represented by constraining the temperature to the observed temperature. The Ekman spiral of the model then shows very good agreement with the observations. However, we do not find any evidence of the Stokes-Coriolis effect, whereas accurate wave hindcasts suggest that it should be significant, leading to upwind transport around 9.5% of the crosswind Ekman transport. The nature of the measurement is then in question, because the bias induced by the waves on near surface measurements from a buoy can be larger than the Stokes transport. Seeking evidence of the Stokes-Coriolis effect such long time averaging, as attempted by *Lewis and Belcher* [2004] and *Polton et al.* [2005], still appears to be feasible but preference should be accorded to measurements from fixed towers or bottom mounted Acoustic Doppler Current Profilers (ADCPs) to get rid of that wave bias.

Finally, we investigated the surface drift predictions of the model in the presence of stratification. It is shown that the wave age effect on the surface drift, which was found to be small in unstratified conditions, is important in the presence of shallow diurnal mixed layers. In such case, considering separately the wave field and the mean current should give significant differences on surface drift predictions.

Acknowledgments. The initial version of the computer code for the mixed layer model was kindly provided by Yign Noh. We acknowledge the National Buoy Data Center (NDBC) and the Upper Ocean Mooring Data Archive of the Woods Hole Oceanographic Institution (WHOI) for their web-available data. N.R. acknowledges the support of a CNRS-DGA doctoral research grant.

References

Agrawal, Y. C., E. A. Terray, M. A. Donelan, P. A. Hwang, A. J. Williams, W. Drennan, K. Kahma, and S. Kitaigorodskii (1992), Enhanced dissipation of kinetic energy beneath breaking waves, *Nature*, *359*, 219–220.

Ardhuin, F., and A. Le Boyer (2006), Numerical modelling of sea states: validation of spectral shapes (in French), *Navigation*, *54*(216), 55–71.

Ardhuin, F., T. H. C. Herbers, K. P. Watts, G. P. van Vledder, R. Jensen, and H. Graber (2007a), Swell and slanting fetch effects on wind wave growth, *J. Phys. Oceanogr.*, *37*(4), 908–931, doi:10.1175/JPO3039.1.

Ardhuin, F., N. Rascle, and K. A. Belibassakis (2007b), Explicit wave-averaged primitive equations using a generalized lagrangian mean, *Ocean Modelling*, in press [http://arxiv.org/abs/physics/0702067].

Beardsley, R. C., E. P. Dever, S. J. Lentz, and J. P. Dean (1998), Surface heat flux variability over the northern california shelf, *J. Geophys. Res.*, *103*, 21 553 –21 586.

Bidlot, J., S. Abdalla, and P. Janssen (2005), A revised formulation for ocean wave dissipation in CY25R1, *Tech. Rep. Memorandum R60.9/JB/0516*, Research Department, ECMWF, Reading, U. K.

Craig, P. D., and M. L. Banner (1994), Modeling wave-enhanced turbulence in the ocean surface layer, *J. Phys. Oceanogr.*, *24*, 2546–2559.

Ekman, V. W. (1905), On the influence of the earth's rotation on ocean currents, *Ark. Mat. Astron. Fys.*, *2*, 1–53.

Garrett, C. (1976), Generation of Langmuir circulations by surface waves - a feedback mechanism, *J. Mar. Res.*, *34*, 117–130.

Gaspar, J. P., Y. Grégoris, and J. M. Lefevre (1990), A simple eddy kinetic energy model for simulations of oceanic vertical mixing : Tests at station papa and long-term upper ocean study site., *J. Geophys. Res.*, *95*(C9), 16,179–16,193.

Hasselmann, K. (1970), Wave-driven inertial oscillations, *Geophys. Fluid Dyn.*, *1*, 463–502.

Hasselmann, K., et al. (1973), Measurements of wind-wave growth and swell decay during the Joint North Sea Wave Project, *Deut. Hydrogr. Z.*, *8*(12), 1–95, suppl. A.

Huang, N. E. (1979), On surface drift currents in the ocean, *J. Fluid Mech.*, *91*, 191–208.

Jenkins, A. D. (1987), Wind and wave induced currents in a rotating sea with depth-varying eddy viscosity, *J. Phys. Oceanogr.*, *17*, 938–951.

Jenkins, A. D. (1989), The use of a wave prediction model for driving a near-surface current model, *Deut. Hydrogr. Z.*, *42*, 133–149.

Kantha, L. H., and C. A. Clayson (2004), On the effect of surface gravity waves on mixing in the oceanic mixed layer, *Ocean Modelling*, *6*, 101–124.

Kudryavtsev, V. N., V. K. Makin, and B. Chapron (1999), Coupled sea surface–atmosphere model. 2. spectrum of short wind waves, *J. Geophys. Res.*, *104*, 7625–7639.

Large, W. G., and S. Pond (1981), Open ocean momentum flux measurements in moderate to strong winds, *J. Phys. Oceanogr.*, *11*, 324–336.

Lentz, S. J., M. Fewings, P. Howd, J. Fredericks, and K. Hathaway (2007), Observations of undertow over the inner continental shelf, *J. Phys. Oceanogr.*, pp. ???–???

Lewis, D. M., and S. E. Belcher (2004), Time-dependent, coupled, Ekman boundary layer solutions incorporating Stokes drift, *Dyn. Atmos. Oceans*, *37*, 313–351.

McWilliams, J. C., and E. Huckle (2006), Ekman layer rectification, *J. Phys. Oceanogr.*, *36*, 1646–1659.

McWilliams, J. C., and J. M. Restrepo (1999), The wave-driven ocean circulation, *J. Phys. Oceanogr.*, *29*, 2523–2540.

McWilliams, J. C., P. P. Sullivan, and C.-H. Moeng (1997), Langmuir turbulence in the ocean, *J. Fluid Mech.*, *334*, 1–30.

Mellor, G. L. (2001), One-dimensional, ocean surface layer modelling: A problem and a solution, *J. Phys. Oceanogr.*, *31*, 790–809.

Monismith, S. G., E. A. Cowen, H. M. Nepf, J. Magnaudet, and L. Thais (2007), Laboratory observations of mean flows under surface gravity waves, *J. Fluid Mech.*, *573*, 131–147.

Noh, Y. (1996), Dynamics of diurnal thermocline formation in the oceanic mixed layer, *J. Geophys. Res.*, *26*, 2189–2195.

Noh, Y. (2004), Sensitivity to wave breaking and the Prandtl number in the ocean mixed layer model and its dependence on latitude, *Geophys. Res. Lett.*, *31*, L23,305, doi:10.1029/2004GL021289.

Noh, Y., and H. J. Kim (1999), Simulations of temperature and turbulence structure of the oceanic boundary layer with the improved near-surface process, *J. Geophys. Res.*, *104*(C7), 15,621–15,634.

Noh, Y., H. S. Min, and S. Raasch (2004), Large eddy simulation of the ocean mixed layer: the effects of wave breaking and Langmuir circulation, *J. Phys. Oceanogr.*, *34*, 720–733.

Polton, J. A., D. M. Lewis, and S. E. Belcher (2005), The role of wave-induced Coriolis-Stokes forcing on the wind-driven mixed layer, *J. Phys. Oceanogr.*, *35*, 444–457.

Price, J. F., and M. A. Sundermeyer (1999), Stratified Ekman layers, *J. Geophys. Res.*, *104*(C9), 20,467–20,494.

Price, J. F., R. A. Weller, and R. R. Schudlich (1987), Wind-driven ocean currents and ekman transport, *Science*, *238*, 1534–1538.

Rascle, N., F. Ardhuin, and E. A. Terray (2006), Drift and mixing under the ocean surface. a coherent one-dimensional description with application to unstrati.ed conditions, *J. Geophys. Res.*, *111*, C03,016, doi:10.1029/2005JC003004.

Rascle, N., F. Ardhuin, P. Queffeulou, and D. Croiz-Fillon (2008), A global wave parameter database for wave-current-turbulence interaction studies, *Ocean Modelling*, in press.

Santala, M. J. (1991), Surface referenced current meter measurements, Ph.D. thesis, Woods Hole Oceanographic Institution and the Massachusetts Institute of Technology, wHOI-91-35.

Schudlich, R. R., and J. F. Price (1998), Observations of seasonal variation in the Ekman layer, *J. Phys. Oceanogr.*, *28*, 1187–1204.

Smith, J. A. (2006), Observed variability of ocean wave Stokes drift, and the Eulerian response to passing groups, *J. Phys. Oceanogr.*, *36*, 1381–1402.

Stramma, L., P. Cornillon, R. A. Weller, J. F. Price, and M. G. Briscoe (1986), Large diurnal sea surface temperature variability : Satellite and in situ measurements, *J. Phys. Oceanogr.*, *16*, 827–837.

Terray, E. A., M. A. Donelan, Y. C. Agrawal, W. M. Drennan, K. K. Kahma, A. J. Williams, P. A. Hwang, and S. A. Kitaigorodskii (1996), Estimates of kinetic energy dissipation under breaking waves, *J. Phys. Oceanogr.*, *26*, 792–807.

Terray, E. A., W. M. Drennan, and M. A. Donelan (2000), The vertical structure of shear and dissipation in the ocean surface layer, in *Proc. Symp. on Air-Sea Interaction, Sydney*, pp. 239–245, University of New South Wales.

Tolman, H. L., B. Balasubramaniyan, L. D. Burroughs, D. V. Chalikov, Y. Y. Chao, H. S. Chen, and V. M. Gerald (2002), Development and implementation of wind-generated ocean surface wave models at NCEP, *Weather and Forecasting*, *17*(4), 311–333.

Xu, Z., and A. J. Bowen (1994), Wave- and wind-driven flow in water of finite depth, *J. Phys. Oceanogr.*, *24*, 1850–1866.

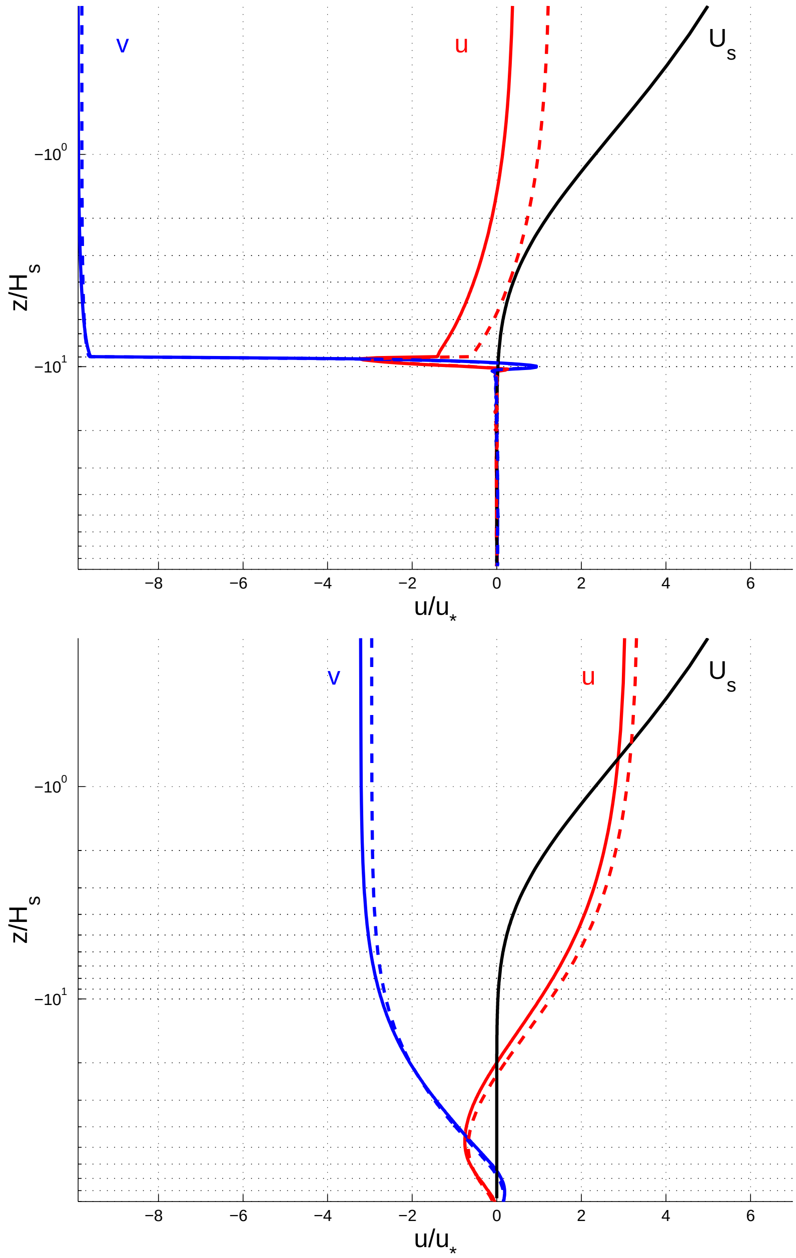

Figure 1. Velocity profiles from the model. $\widehat{u}$ is the downwind quasi-Eulerian velocity, $\widehat{v}$ is the crosswind quasi-Eulerian velocity and U_s is the Stokes drift. Velocities and elevation are normalized by the waterside friction velocity u_* and by the significant wave height H_s, respectively. Solid lines and dashed lines are model results with and without the Stokes-Coriolis effect, respectively. Upper panel is with a 20 m deep mixed layer as observed during SMILE and lower panel is without the effect of stratification.

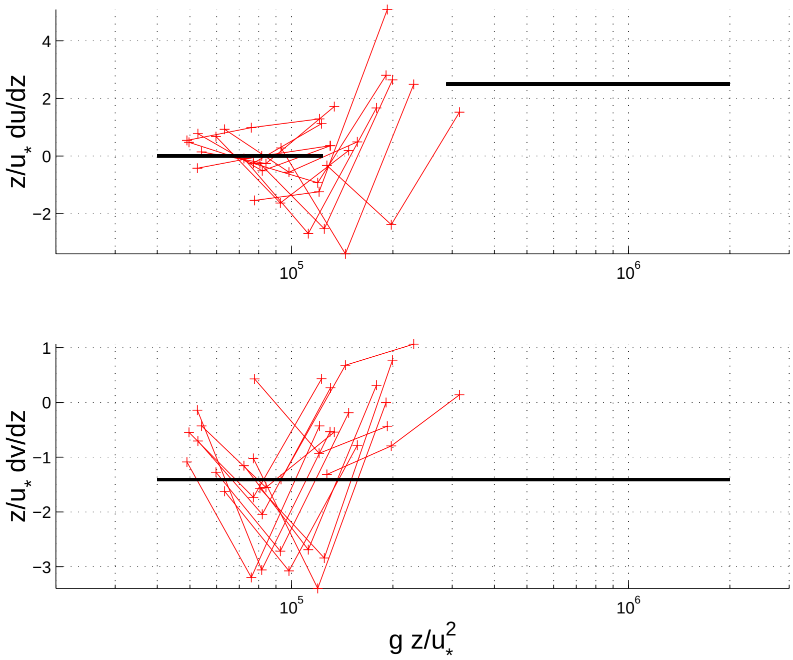

Figure 2. Reproduction of the Figure 7-5 of *Santala* [1991], for the SASS data only. Nondimensional variation of shear with depth for the downwind (upper panel) and for the crosswind (lower panel) directions. The + and thin lines are measurements from the SASS, the thick solid lines are the shears inferred in the original analysis of *Santala* [1991], with the 3 layers structure in the downwind direction.

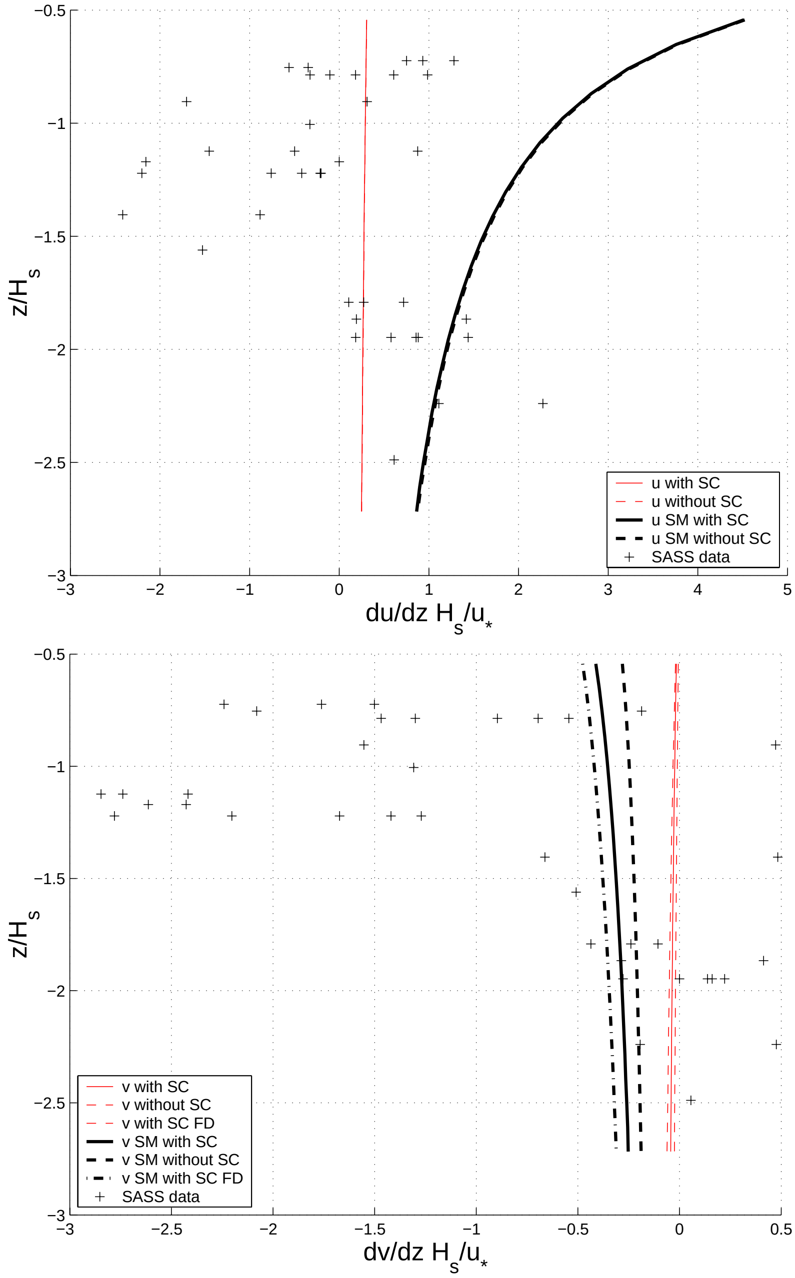

Figure 3. (Upper panel) Shear of the downwind component u of the current, normalized with u_*/H_s, plotted as function of the depth normalized with H_s. Shears of the model are calculated by finite difference and shears of the SASS data are calculated by finite difference between each pairs of adjacent sensors. In addition to the default model results, we plotted the results of the model without the Stokes-Coriolis effect (SC) or/and without the wave-induced surface mixing (SM= Small Mixing), obtained with a roughness length of $z_0 = 0.05$ m and no TKE surface flux. (Lower panel) Same as upper panel but for the crosswind component v of the current. As an upper bound of the Stokes-Coriolis effect, the model results when supposing the wave field fully developed (FD) is also shown.

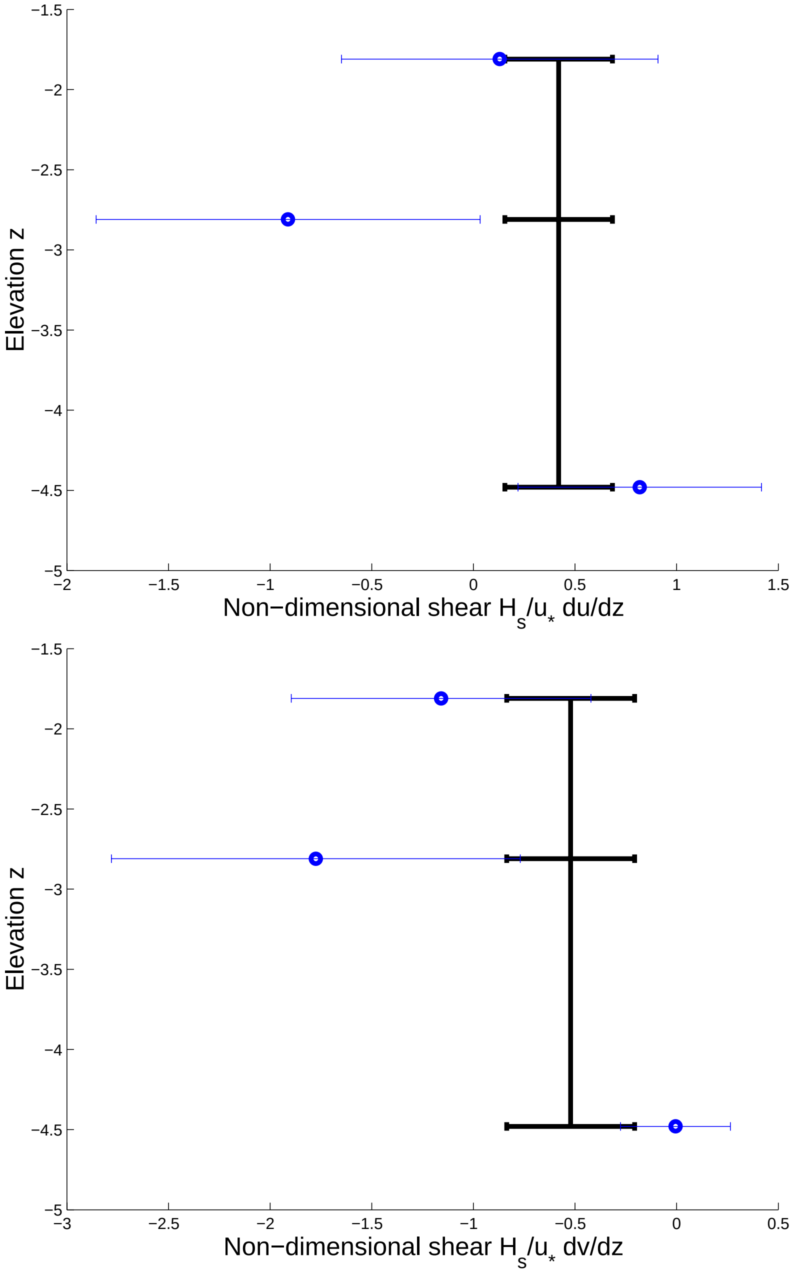

Figure 4. (Upper panel) Shear of the downwind component u of the current, normalized with u_*/H_s, plotted as function of the depth. Dots are shears calculated by finite difference between each pairs of adjacent sensors. Thick line is shear obtained from linear interpolation of the current velocities over the 4 current-meter depths. We show mean values over the set of 13 measurements with error bars representing standard deviations. (Lower panel) Same as upper panel but for the crosswind component v of the current.

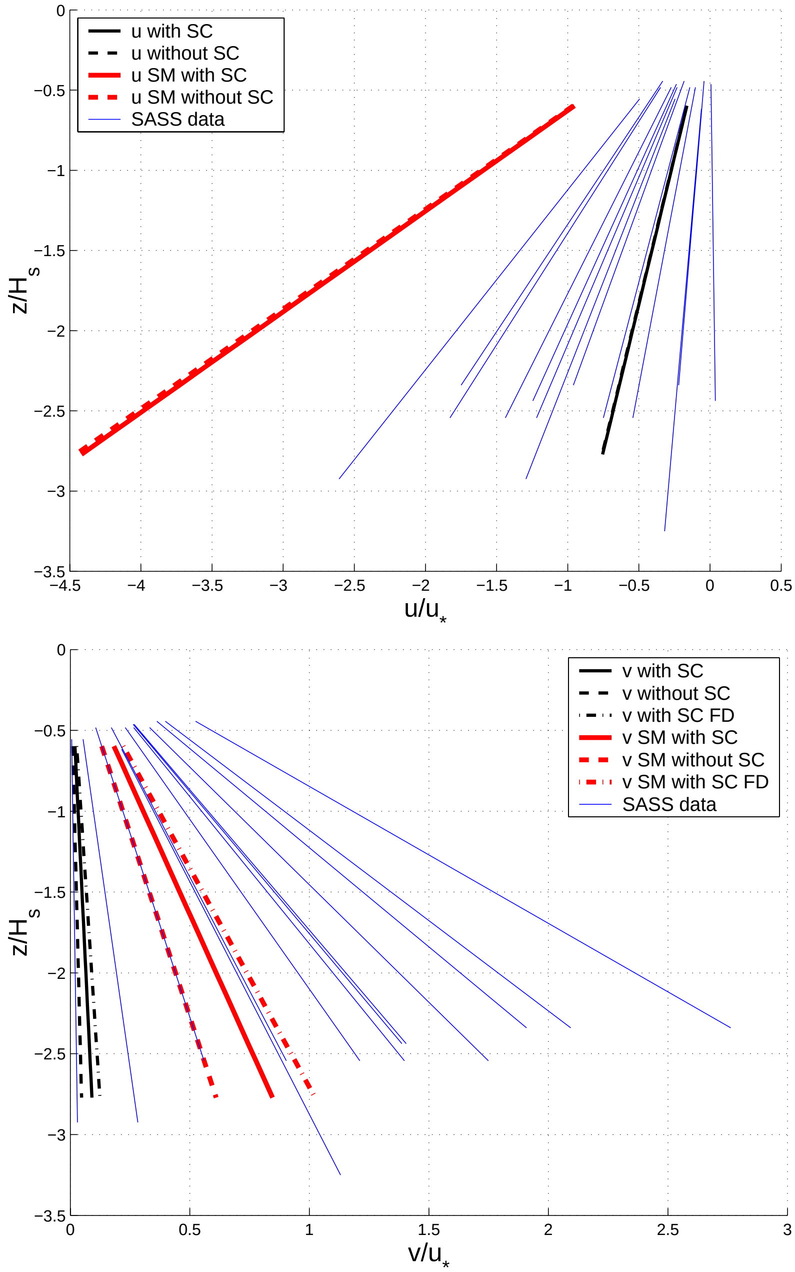

Figure 5. (Upper panel) Linear regression of the downwind current u between 1.1 m and 5.8 m deep, the measurement depths of the SASS buoy. The current is normalized with u_* and the depth with H_s. The SASS data are plotted, as well as different model results. In addition to the default model results, we plotted the results of the model without the Stokes-Coriolis effect (SC) or/and without the wave-induced surface mixing (SM= Small Mixing), obtained with a roughness length of $z_0 = 0.05$ m and no TKE surface flux. (Lower panel) Same as upper panel but for the crosswind component v. The SASS data are plotted, as well as different model results. (As in fig 3, lower panel, SC is Stokes-Coriolis, SM is Small Mixing and FD is Fully Developed waves.)

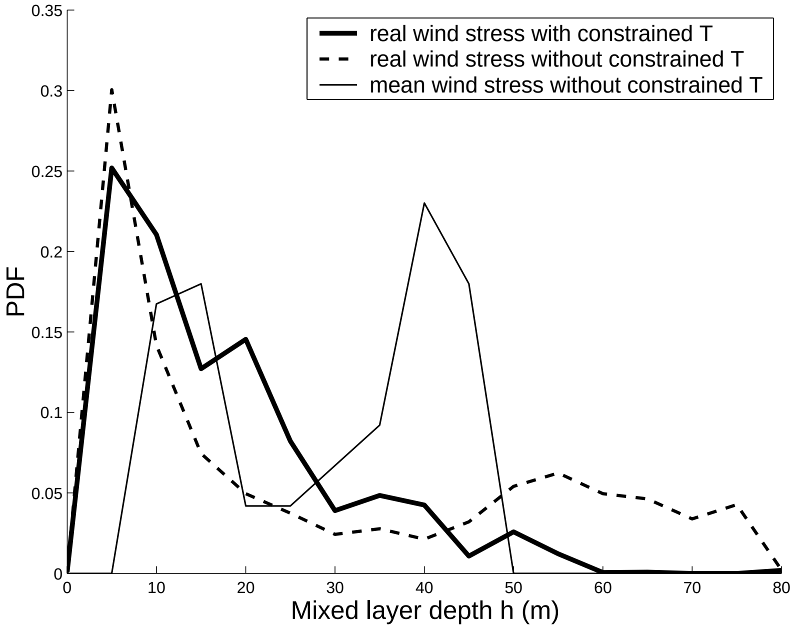

Figure 6. Probability density functions of the hourly mixed layer depth of 3 numerical simulations of the LOTUS 3 measurement. The mixed layer depth is defined with a criteria on attenuation of surface TKE [*Noh*, 2004]. All model runs use the analytical heat flux (15), which closes the heat budget. Thin solid line is the model with the mean observed wind stress (section 4.1), dashed line is with the observed variable wind (section 4.2), thick solid line is with the observed wind and with the temperature assimilation (section 4.3).

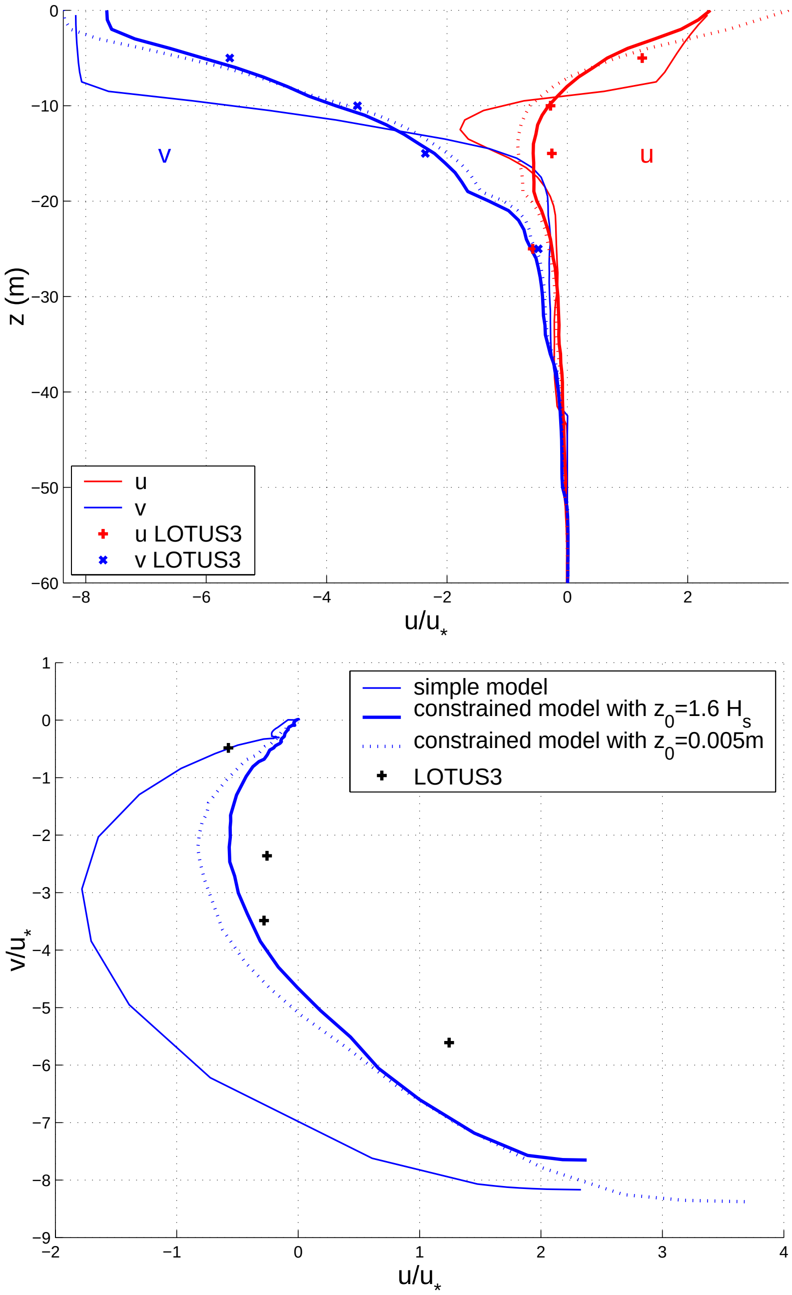

Figure 7. Results of 3 different LOTUS 3 simulations, each without the Stokes-Coriolis force. Upper panel shows vertical profiles of the mean current $(\widehat{u}, \widehat{v})$. Lower panel shows hodographs of the mean current. Each simulation uses the analytical heat flux (15). Thin line uses the mean wind stress (section 4.1). Thick solid and dotted lines use the variable wind stress and the constrained temperature (section 4.3), and test the sensitivity to the the wave-induced mixing with roughness lengths $z_0 = 1.6 H_s$ and $z_0 = 0.005$ m, respectively.

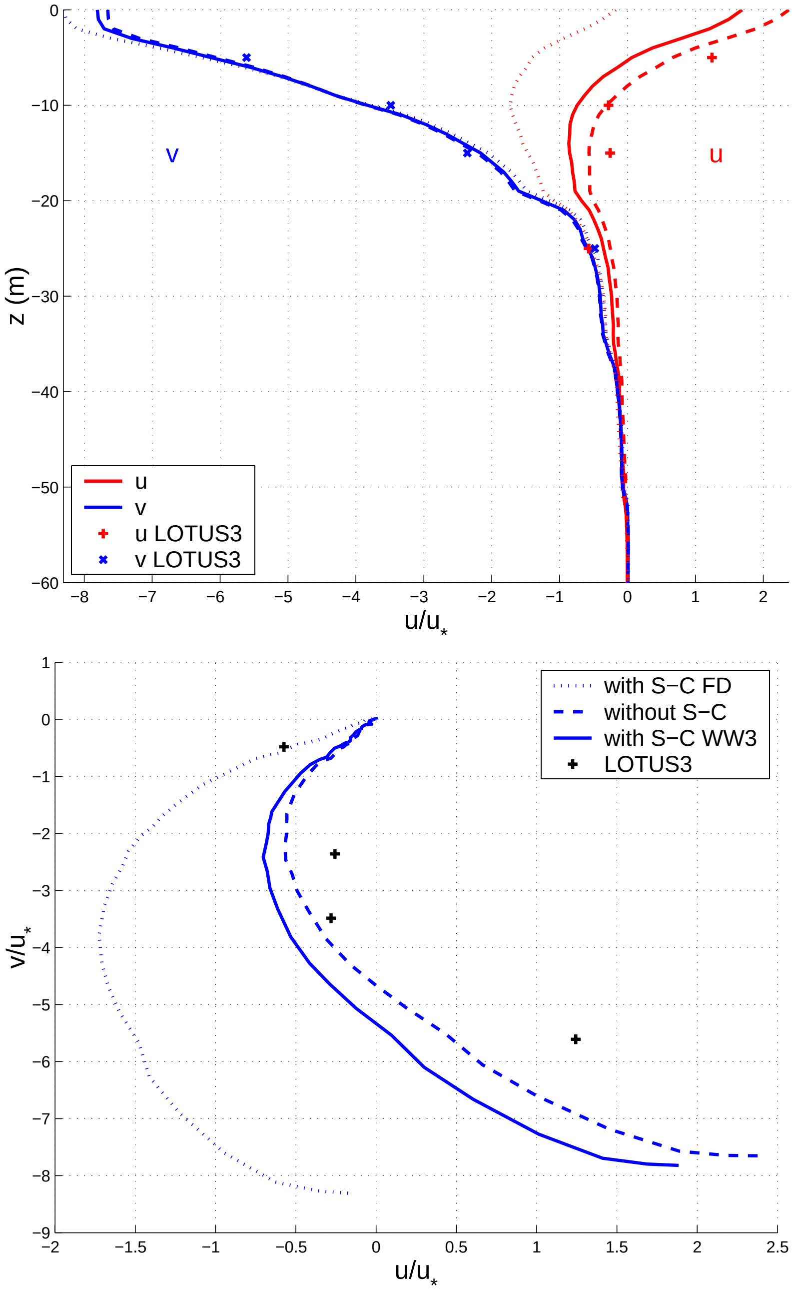

Figure 8. Results of the LOTUS 3 simulation, with the observed wind stress and with the temperature constrained to the data. Upper panel shows vertical profiles of the mean current $(\widehat{u}, \widehat{v})$. Lower panel shows hodographs of the mean current. Dashed lines are the model results without the Stokes-Coriolis effect. Dotted lines are the model results when supposing the waves fully developed (with the 6 hours low-pass filtered wind), giving an upper bound of the Stokes-Coriolis effect. Solid lines are the models results with the Stokes-Coriolis effect calculated with WW3.

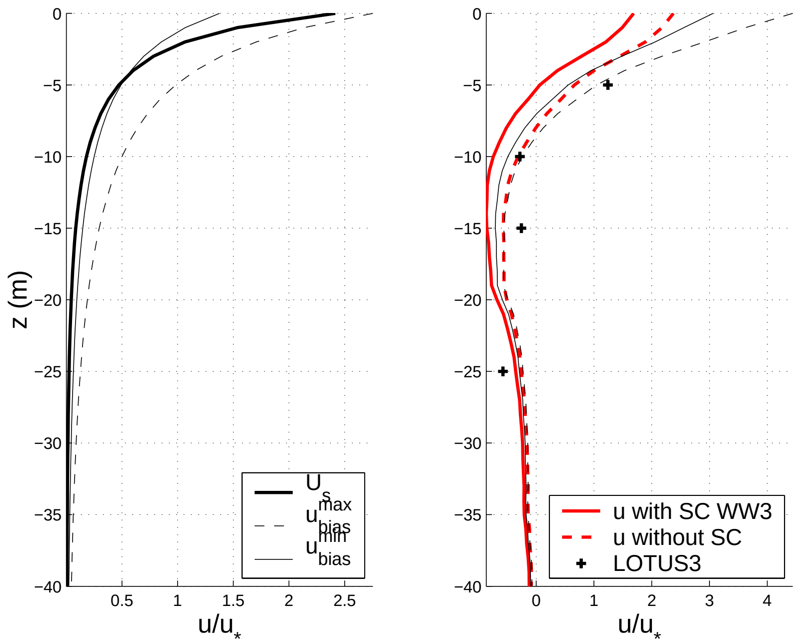

Figure 9. Simulation of the impact of the wave bias on the LOTUS 3 measurements. (Left panel) Vertical profiles of the averaged norm of the Stokes drift U_s (thick solid line), of u_{bias}^{max} (thin dashed line) and of u_{bias}^{min} (thin solid line). (Lower panel) Profile of velocity $\widehat{u}$ calculated with the Stokes-Coriolis effect from the wave reanalysis (thick solid line, similar to fig. 8), augmented with the additional bias u_{bias}^{min} (thin solid line) and u_{bias}^{max} (thin dashed line). Also shown is the velocity $\widehat{u}$ calculated without the Stokes-Coriolis effect (thick dashed line, similar to fig. 8).

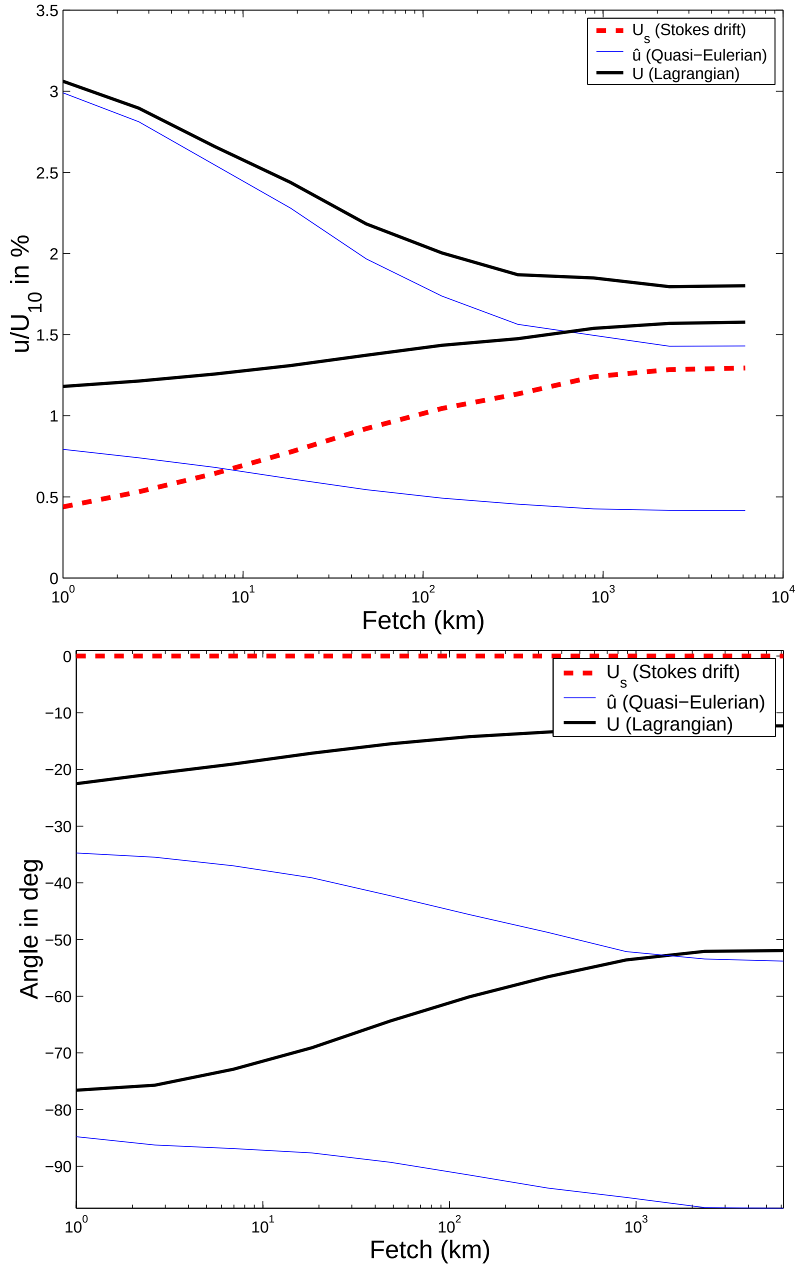

Figure 10. (Upper panel) Stokes drift $\mathbf{U}_s$, quasi-Eulerian current $|\widehat{\mathbf{u}}|$ and total Lagrangian drift $\mathbf{U} = |\widehat{\mathbf{u}} + \mathbf{U}_s|$ at the surface ($z = -0.5$ m), as function of fetch. The velocities are expressed as a percentage of the wind speed U_{10}. The wind is set to $U_{10} = 10\text{ms}^{-1}$, and two different stratifications are obtained from an initially uniform density and applying two different surface heat fluxes, $Q_h = 0$ and $Q_h = 1000$ W m^{-2}. (Lower panel) Angles of deviations from the wind direction, measured counterclockwise, of the quasi-Eulerian current and of the Lagrangian drift.